Seismic reservoir characterization of Duvernay shale with quantitative interpretation and induced seismicity considerations — A case study

Satinder Chopra[1], Ritesh Kumar Sharma[1], Amit Kumar Ray[2], Hossein Nemati[1], Ray Morin[3], Brian Schulte[3], and David D'Amico[3]

Abstract

The Devonian Duvernay Formation in northwest central Alberta, Canada, has become a hot play in the past few years due to its richness in liquid and gaseous hydrocarbon resources. The oil and gas generation in this shale formation made it the source rock for many oil and gas fields in its vicinity. We attempt to showcase the characterization of Duvernay Formation using 3D multicomponent seismic data and integrating it with the available well log and other relevant data. This has been done by deriving rock-physics parameters (Young's modulus and Poisson's ratio) through deterministic simultaneous and joint impedance inversion, with appropriate quantitative interpretation. In particular, we determine the brittleness of the Duvernay interval, which helps us determine the sweet spots therein. The scope of this characterization exercise was extended to explore the induced seismicity observed in the area (i.e., earthquakes of magnitude >3 M) that is perceived to be associated with hydraulic fracture stimulation of the Duvernay. This has been a cause of media coverage lately. We attempt to integrate our results with the induced seismicity data available in the public domain and elaborate on our learning experience gained so far.

Introduction

The Duvernay shale in Alberta, Canada, has been the source rock for many of the larger Devonian oil and gas fields in Alberta (Mossop and Shetsen, 1994), including the oil- and gas-producing Leduc and Nisku Formations. It is often compared with the prolific Cretaceous Eagle Ford Formation of Texas because both shale plays offer a full range of hydrocarbons, from dry gas through liquids-rich gas or condensate to oil. In the past few years, oil and gas companies have scrambled to get acreage over the Duvernay and pick up sweet spots for production. The area of focus in this study is located in the Kaybob and Fox Creek areas of west central Alberta, which is approximately 250 km northwest of Edmonton (Figure 1). In and around the Kaybob area, the Duvernay shale lying at a depth of 3000–3500 m is sufficiently mature and charged with liquids-rich gas to make it economically attractive. Besides thermal maturity, there are other favorable key elements such as richness, thickness and type of organic material in the rock, the reservoir quality, depth, and pressure, which when combined define the so-called sweet spots in the Duvernay liquids-rich formation. It has an effective porosity of 6%–7%, an average vitrinite reflectance (Ro) of 1.12%, an average total organic carbon content of up to 4.5%, an average permeability of 394 nD, an average thickness of approximately 55 m, and high initial pressure, which is favorable for production. The cost of drilling and completion has gradually fallen over the past few years with increased efficiency and enhanced production, with tightly spaced fracs and longer horizontal wells (approximately 2 km) becoming the norm. All in all, the Duvernay has become an established shale play that holds 443 Tcf of natural gas, 11.3 billion bbls of natural gas liquids, and 61.7 billion bbls of oil, per a 2012 report by Alberta Geological Survey.

The main goal for shale resource characterization is usually the identification of these sweet spots that represent the most favorable drilling areas. For this study, the available 3C3D seismic data were acquired in early 2015. After processing, they were made available for reservoir characterization and quantitative interpretation late last year. This seeks to quantify the reservoirs by understanding their elastic properties, lithology, fluid content, and geometric distribution. Such quantification can be carried out by way of P- and S-impedance determination, combined with petrophysical parameters available at the location of the wells. Good well control is critical, but in some cases it is not available. Attempts

[1]Arcis Seismic Solutions, TGS, Calgary, Alberta, Canada. E-mail: schopra@arcis.com; rsharma@arcis.com; mnemati@arcis.com.
[2]Formerly at Arcis Seismic Solutions, TGS, Calgary, Alberta, Canada; presently Pandit Deendayal Petroleum University, Gujarat, India. E-mail: amit.ray77@gmail.com.
[3]Repsol Oil and Gas Canada, Calgary, Alberta, Canada. E-mail: rmorin@repsol.com; bschulte@repsol.com; ddamico@repsol.com.
Manuscript received by the Editor 4 August 2016; revised manuscript received 14 December 2016; published online 27 February 2017; corrected version published online 8 May 2017. This paper appears in *Interpretation*, Vol. 5, No. 2 (May 2017); p. T185–T197, 17 FIGS., 1 TABLE.
http://dx.doi.org/10.1190/INT-2016-0130.1.

at quantitative interpretation of seismic data can result in considerable value addition, which is the goal for this case study. A workflow for performing quantitative seismic interpretation (Chopra, 2015) for the Duvernay shale was chalked out with the following steps. Care was taken to carry out more detailed analysis at each step so that it resulted in value addition to the overall analysis.

Well-log correlation

The Duvernay shale is fine-grained and silica-rich shale unit, which is overlaid by the Ireton (calcareous) and Winterburn shale units, over which lies the Wabamun limestone unit. The Duvernay unit is underlain by a thin carbonate-rich shale layer that overlies the Swan Hills reefal unit. The simplified seismic-based stratigraphic column shown in the left of Figure 2 illustrates these units. In the same figure, we see the correlation of P-velocity, density, and gamma-ray curves (Figure 2a), and the synthetic seismogram (Figure 2b) with stacked data (Figure 2c). A zero-phase wavelet (shown on the top in Figure 2) was estimated from the seismic data using a statistical process. We notice a good correlation overall, except in the highlighted zone, which is above our unit of interest.

Preconditioning of seismic data

The seismic data (PP and PS) were conditioned carefully to make sure that amplitudes are preserved such that their variation with offset/angle could be used in a meaningful way. The major processes used in the conditioning were supergathering (3×3), band-pass filtering, random noise attenuation, and trim statics, with difference plots taken at each step to ensure that no useful signal was distorted or attenuated (Hunt et al., 2015; Chopra and Sharma, 2016). In Figure 3, we show a modeled PP elastic gather being compared with the real seismic gather before and after conditioning. We notice the enhancement in the signal-to-noise ratio after conditioning. At the location of the Swan Hills level, which happens to be a strong positive reflection, the amplitude variation with offset is also shown: the red points indicating the amplitude values for the modeled gather, the blue points coming from the input seismic gather, and the pale yellow points from the same gather after conditioning. The mean trend curves are maintained even as the data scatter is reduced, and the zero-offset amplitudes for the modeled and the conditioned gathers are very close. Similar conditioning was undertaken for the PS seismic gathers.

Figure 1. Location of 3D seismic data in the Fox Creek study area, Alberta, Canada (image generated using Google Earth).

The PP gathers were picked up first for running simultaneous inversion, which was followed by joint inversion, post and prestack.

A time horizon corresponding to the Swan Hills marker is shown in Figure 4, wherein the four well locations have been marked. The diagonal linear pattern seen in the middle of the display corresponds to the termination of the Swan Hills reef trend that is widely spread out to the right, and the region to the left of this trend is devoid of any shoaling.

Low-frequency trend determination for impedance inversion

While carrying out impedance inversion, the addition of a low-frequency trend is necessary for obtaining absolute values of impedance. The usual practice is to low-pass filter (<10 Hz) the available impedance well-log curves and use one or more of the derived curves for generation of the low-frequency trend volume using extrapolation or interpolation and guided by horizon boundaries. When more than one well is used for the generation of the low-frequency trend, usually an inverse-distance weighted scheme or a process called kriging is used. Such techniques need to be used with care because they can produce artifacts. We instead make use of a relatively new approach for this low-frequency trend generation, which considers well-log data and seismic data to establish a relationship between seismic attributes and the available well-log curves. Using the low-frequency model generated with a single well as one of the inputs and some other seismic data volumes (relative acoustic impedance, instantaneous amplitude, dominant frequency, filtered seismic [10–20–30–40 and 10–20–50–60 Hz]), a multiregression approach (Ray and Chopra 2015, 2016) is used, wherein a target log is modeled as a linear combination of several input attributes at each sample point. This results in a series of linear equations that are solved by obtaining a linear-weighted sum of the input seismic attributes in such a way that the error between the predicted and the target log is minimized. The choice of the different seismic attributes used could vary, but for the case at hand, we have used the relative acoustic impedance, some instantaneous attributes, and different versions of the filtered seismic data as inputs. Cross validation of the predicted attributes forms part of the workflow, in which one well is withdrawn and is estimated using the other wells and compared. If the cor-

relation coefficient between the existing and predicted curves is high, which was found to be the case, it lends more confidence to the analysis.

Figure 5a shows a comparison of the predicted or generated low-frequency P-impedance trend using multiregression analysis with the filtered low-frequency impedance curve for well W-3. The two seem to match reasonably well. In Figure 5b, we show the horizon slice display at the Duvernay level from the lower frequency impedance volume. Notice the gradual change between the northwest and southeast quadrants, perhaps reflecting the Swan Hills trend below this level. In Figure 5c, we do see a distinct change reflecting the Swan Hills trend as expected. Similar low-frequency models are generated for the S-impedance and density as well.

Simultaneous inversion

In simultaneous prestack inversion, multiple partial-offset or angle substacks are inverted simultaneously. For each angle stack, a unique wavelet is estimated. Subsurface low-frequency models for P-impedance, S-impedance, and density constrained with appropriate horizons

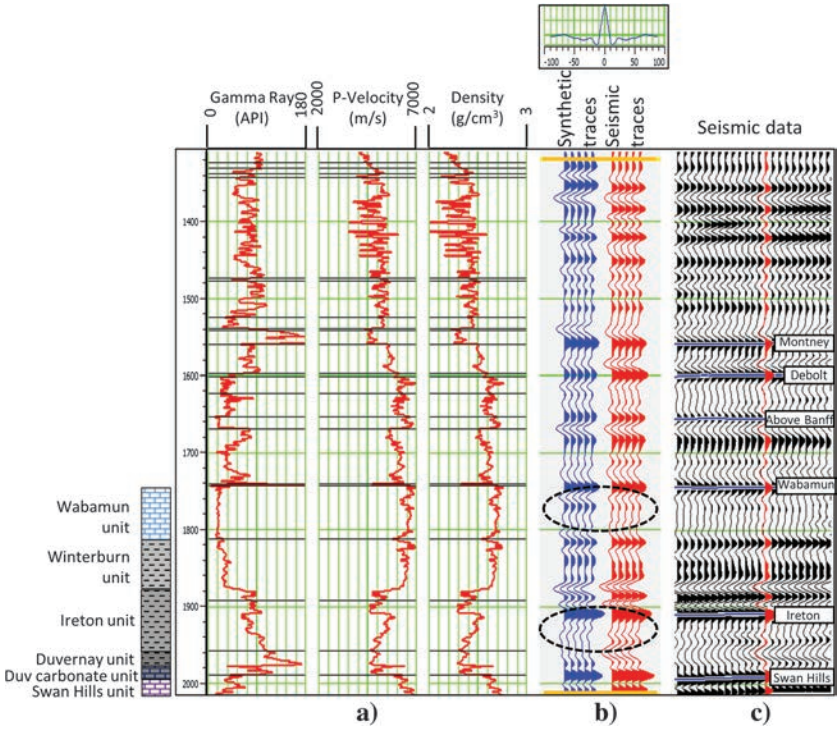

Figure 2. Correlation of W-2 well-log curves with seismic data. The blue traces represent the synthetics (generated with the wavelet shown above), whereas the red traces represent the seismic data. The correlation coefficient between the synthetic and red traces in the time window indicated by the yellow bars is 0.82, suggesting an overall good correlation (data courtesy of Arcis Seismic Solutions, TGS, Calgary).

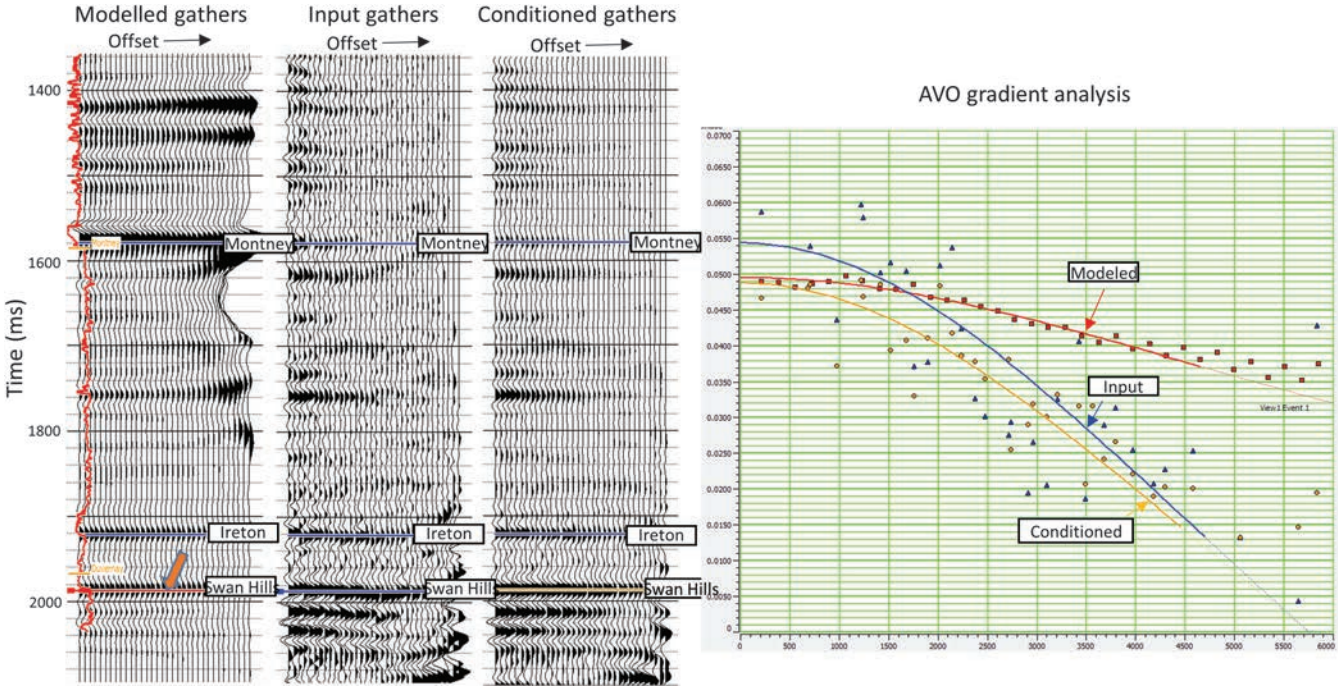

Figure 3. Comparison between modeled gathers at the location of well W-3, and the equivalent input gathers, and conditioned gathers, as well as the amplitude analysis at the Swan Hills event (orange arrow). The scatter of points after conditioning (in yellow) is reduced (data courtesy of Arcis Seismic Solutions, TGS, Calgary).

in the broad zone of interest are constructed using the approach explained above. The models, wavelets, and partial stacks were used as input in the inversion, and the output was P-impedance and S-impedance.

Joint inversion

Inversion of P-wave data together with S-wave data is referred to as joint inversion. Joint inversion makes use of the amplitudes and traveltimes of the P-wave and S-wave data for estimating P-impedance, S-impedance, and density to provide a more robust inversion result. The main advantage of using 3D3C data is that the large angle range requirement for density determination from PP data gets relaxed; the PS data reflection data are reflected at steeper angles at the common conversion points (Lawton, 1991). Therefore, this leads to a more robust density determination.

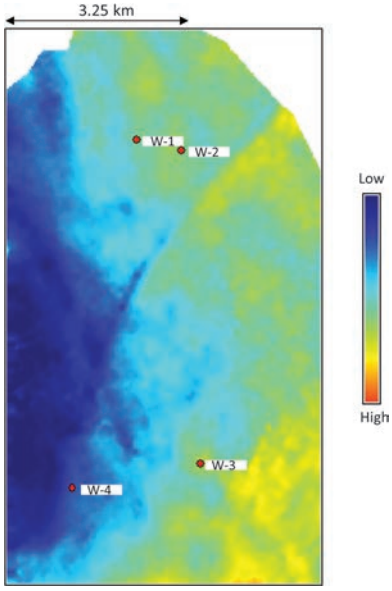

Figure 4. Time horizon picked at the Swan Hills level with the location of four wells overlaid (data courtesy of Arcis Seismic Solutions, TGS, Calgary).

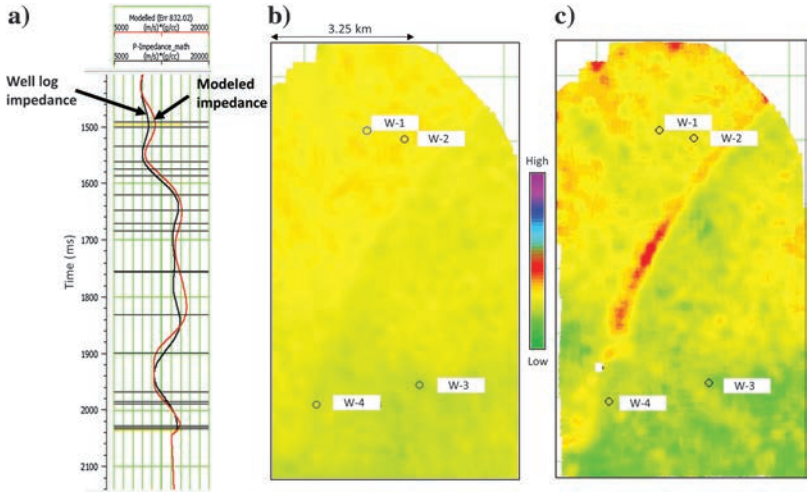

Figure 5. (a) Prediction of low-frequency P-impedance trend for blind well W-3 using multiattributes regression analysis and its comparison with the real P-impedance well-log curve; (b) horizon slice from the low-frequency trend volume at the (b) Duvernay and (c) Swan Hills level. Notice the gradual variation of P-impedance seen on the slice at the Duvernay level, and a distinct change reflecting the Swan Hills trend as expected (data courtesy of Arcis Seismic Solutions, TGS, Calgary).

After processing of multicomponent seismic data, the outputs are PP-wave data processed in PP two-way time and PS-wave data processed in PS time scale. For continuing any consistent analysis, the next step is to perform an accurate PP and PS time correspondence, which is accomplished by tying with PP and PS synthetic seismograms, respectively, generated over the same range of frequency bandwidth as the input reflection data. This process is referred to as registration. It is usually done by matching the corresponding correlative events on the PP and PS data volumes and then mapping or shrinking the PS time scale to the PP time scale. In Figure 6, we show the well-to-seismic correlation for PS data at well W-3. The well-log curves are shown in Figure 6a, and the PS synthetic seismogram (blue traces) correlation with real PS seismic data (red traces) is seen in Figure 6b. The correlation between the two was found to be 93%, which is very encouraging. A segment of the PS data in PS time is shown in Figure 6c.

Once the well-to-seismic correlation for PP and PS data is done satisfactorily, the depth-time curves for both are determined. The V_P/V_S ratio determined this way is valid at the location of the well only. Using this information, the PP data with its horizons (in blue) are stretched to PS time and displayed alongside PS data (in PS time) as in Figure 6d. This helps in identifying the corresponding horizons on the PS data; the trackable horizons are then picked as shown in magenta (Figure 6c). The horizons picked on PP and PS data will match at the location of the wells but laterally may exhibit traveltime differences. Such differences are determined for the various intervals bounded by horizons, and V_P/V_S ratios are determined for those intervals as per the equation below:

$$\frac{V_P}{V_S} = 2\left(\frac{\text{PS isochron}}{\text{PP isochron}}\right) - 1. \quad (1)$$

In Figure 7, we show a horizon slice from the V_P/V_S volume generated at the Duvernay level via the PP-PS registration. The variation of the V_P/V_S values was confirmed at a few blind wells, and so it was taken to be accurate. Joint inversion can be carried out with poststack as well as prestack multicomponent seismic data. For poststack joint inversion, the inputs are the PP stacked data, the PS stacked data, the wavelets extracted from the two data sets in the

broad zone of interest, and the P-impedance and S-impedance models. Although the PP stack is the normal incidence data, PS data may be taken as the stack at say 12° or 15°, in which the mode conversion sets in. The reflectivities modeled at 0° and 15° and convolved with the appropriate wavelets are compared with the real PP and PS seismic data and the error between them is minimized in a least-squares sense. In the case of prestack joint inversion, usually three or five angle-limited stacks are first generated. Modeled reflectivities at these angles are generated, compared with the real data, and the error is then iteratively minimized in a least-squares sense. In each case, the output from joint inversion was P-impedance, S-impedance, and density data (Chopra and Sharma, 2015).

Equivalent segments of P-impedance sections passing through well W-3 from simultaneous, poststack joint, and prestack joint inversion are shown in Figure 8. The impedance log curve filtered to seismic bandwidth is overlaid on the individual sections, in the form of a curve as well as a colored strip. The correlation between the well impedance and the inverted impedance looks good; we do not expect drastic differences between the P-impedance computations from the three different methods. Because the usable angle range for simultaneous inversion was up to only 35°, a useful density attribute could not be derived therefrom. The density was instead forthcoming from poststack and prestack joint inversion. A comparison of horizon slices averaged from 5 to 20 ms above the Swan Hills marker, which is essentially the Duvernay zone, is shown in Figure 9. One can make out various spatial differences between them, but a greater level of detail is seen on the density slice from the prestack joint inversion display. Although the density values at wells W-2, W-3, and W-4 seem to be close on the two displays, those at wells W-1 are different and close to the actual density log value.

Impedance inversion analysis

The P- and S-impedance volumes obtained from the different types of inversion were again subjected to QC checks at the blind well locations and then put through rock-physics analysis on the derived attributes. A common QC is to crossplot the log-derived P- and S-impedance values at the different wells against the seismic-derived impedance values at those locations. One such representative crossplot is shown in Figure 10, and a correlation comparison coefficient comparison for different inversion methods is exhibited in Table 1. Notice that the correlation coefficients increase as we go from simultaneous inversion to prestack joint inversion, which is what is expected from multicomponent seismic data in terms of value addition.

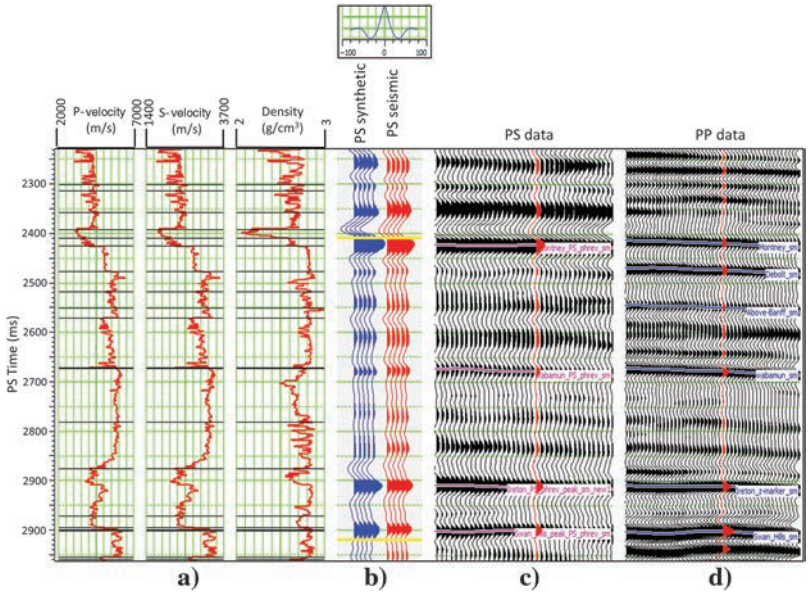

Figure 6. Well-to-seismic correlation for PS data as well as registration with PP data, at well W-3. The PS synthetic seismogram (blue traces) is shown in (b) correlated with PS real seismic traces (in red). The displayed wavelet, used for generation of the synthetic seismogram, was extracted from the PS seismic data using a statistical process. The PS (c) and PP data (d) are shown in PS time (data courtesy of Arcis Seismic Solutions, TGS, Calgary).

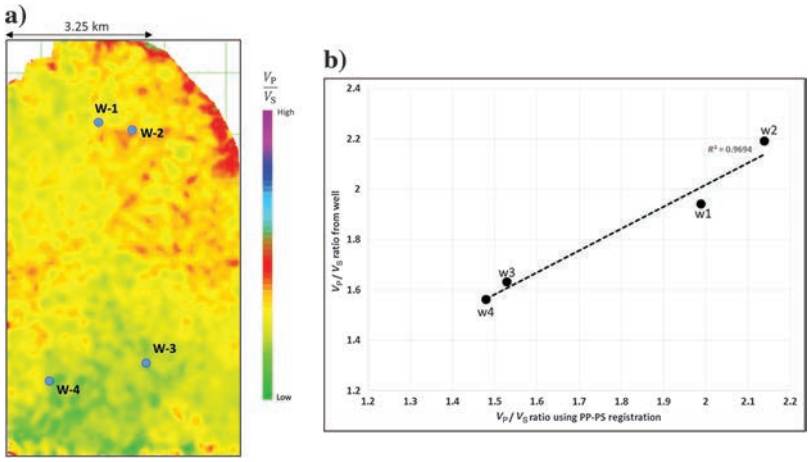

Figure 7. (a) Horizon slice at the Duvernay level from the V_P/V_S volume generated via the PP-PS registration. The variations of V_P/V_S values seem to correlate well with the respective values at the well locations, as can be seen in (b), which shows a crossplot of V_P/V_S computed from well-log data as well as that derived from PP-PS registration (data courtesy of Arcis Seismic Solutions, TGS, Calgary).

Brittleness determination of the Duvernay

Besides other favorable considerations that are desired of unconventional reservoirs, such as shale resource formations, it is vital that reservoir zones are sufficiently brittle. Brittle zones fracture better as is required for higher production. Among the different physical parameters that characterize the rocks, Young's modulus E is a measure of brittleness. Attempts are usually made to determine this physical constant from well-log data but such measurements are localized over a small area. For studying lateral variation of brittleness across an area, 3D seismic data provide a solution. Computation of Young's modulus from seismic data requires the density attribute from inversion, which generally is viewed with suspicion with regard to its stability. A new attribute ($E\rho$) in the form of a product of Young's modulus and density has been introduced (Sharma and Chopra, 2015). For a brittle rock, the Young's modulus and density are expected to be high, and so, the $E\rho$ attribute would exhibit a high value and serve as a brittleness indicator. As well, the new attribute may be used for lithofluid detection, when it is used in conjunction with the product of bulk modulus and density.

In Figure 11, we show a crossplot between E-rho and Poisson's ratio for well W-1 covering data from a broad zone including the Duvernay interval. Both attributes were filtered to the bandwidth of the seismic data. The cluster of points enclosed in the red polygon look anomalous and on back-projection to the log curves is found to come from the Duvernay zone.

Encouraged by the W-1 log crossplot, the same two attributes derived from prestack joint inversion for the same time interval were crossplotted as shown in Figure 12. Again, we see a similar structure of the cluster of points. The anomalous looking points are enclosed in a red polygon and back-projected on the vertical seismic section. It highlights areas on the vertical section that exhibit higher brittleness.

Alternatively, a different brittleness index or average attribute volume was also generated. Grieser and Bray (2007) show that brittleness average can be computed from Young's modulus and Poisson's ratio as

$$\text{brittleness index} = \frac{E_B + \upsilon_B}{2}, \tag{2}$$

where

$$E_B = \frac{(E - E_{min})}{(E_{max} - E_{min})}, \quad \text{and} \quad \nu_B = \frac{(\nu - \nu_{max})}{(\nu_{min} - \nu_{max})},$$

$$\text{brittleness index} = \frac{E * \text{rho} - E * \text{rho}_{min}}{2(E * \text{rho}_{max} - E * \text{rho}_{min})} + \frac{(\nu - \nu_{max})}{2(\nu_{min} - \nu_{max})}. \tag{3}$$

Following this approach, we computed the brittleness average volume and then generated a strata slice at the Duvernay level by averaging the attribute over a small time interval (10 ms). Pockets with high values

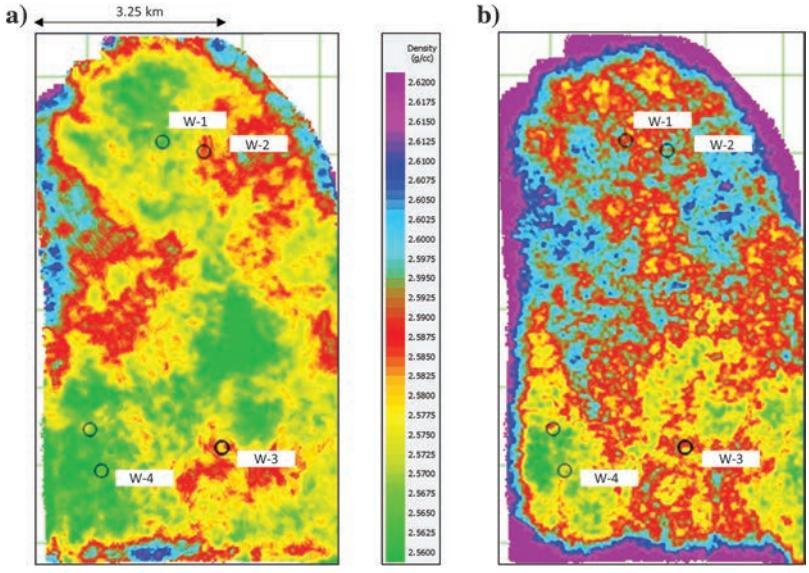

Figure 9. Horizon slices averaged from 5 to 20 ms above the Swan Hills marker that is essentially the Duvernay zone, from (a) simultaneous inversion, (b) joint poststack inversion, and (c) prestack joint inversion (data courtesy of Arcis Seismic Solutions, TGS, Calgary).

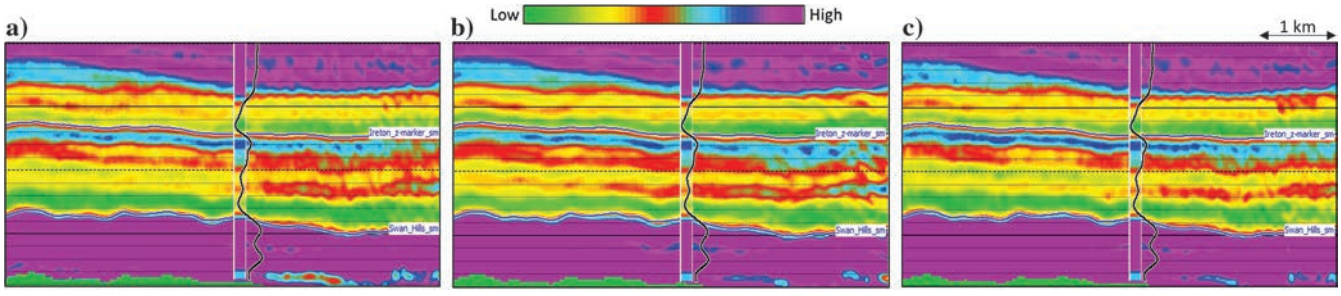

Figure 8. Segment of a section from the impedance volume generated by (a) using simultaneous inversion, (b) poststack joint inversion, and (c) prestack joint inversion. Impedance curve for well W-3 filtered to the seismic bandwidth is shown overlaid on each of the sections (data courtesy of Arcis Seismic Solutions, TGS, Calgary).

of brittleness are indicated in purple color. It should be mentioned here that the density attribute could have been used and the brittleness index computed using equation 2, but we instead used equation 3 for brittleness. We will revisit this example in the next section.

Induced seismicity in the Fox Creek area

The Fox Creek area in Alberta has been in the news recently due to two earthquakes at or above 4 Mw (moment magnitude). A recent study (Atkinson et al., 2016) suggests that approximately 0.3% of frac wells in the WCSB may be correlated with cases of induced seismicity ≥ 3 M, and the common perception is that in the Fox Creek area, they are triggered by hydraulic fracturing (HF) of the Duvernay Formation. Because pipelines, oil and gas wells, and structures at HF sites are potentially vulnerable to the effects of large seismicity, the Alberta Energy Regulator (AER, 2016) is taking the issue seriously.

If the seismicity data that have been collected in Alberta by Composite Alberta Seismicity Catalog (CASC) are examined, especially from 1906 to 2013, one finds sparsely occurring and very feeble magnitude events in the province. In contrast, if the data collected between 2014 and 2015 are examined, one notices weak-magnitude seismicity clusters in and around areas of some HF operations, such as Fort St. John, Fox Creek, and Turner Valley, to name a few.

Similarly, Oklahoma has also been in the news regarding induced seismicity but generated instead by wastewater injection. A recent report (Weingarten et al., 2015; Kutchment, 2016) has concluded that the rate of earthquakes has sharply increased from human activity. Other US states, such as Colorado, New Mexico, Texas, Arkansas, Kansas, and Ohio, have recorded seismicity due to wastewater disposal.

Injection of fluid, whether by HF or wastewater disposal, will result in higher interstitial pressure or pore pressure, which beyond the cracking of rock may result in reactivating already existing fractures or faults. Induced seismicity as such is a well-known phenomenon caused by *mining*, *reservoir*, or *dam impoundment* and *water injection*.

Hydraulic fracture stimulation associated with the creation of new fractures and certain kinds of interaction with preexisting fractures, normally results in small-magnitude "microseismicity." The magnitudes can vary with the location and hydraulic energy but are generally < +1 M to −3 M, too weak to be recorded at the surface except by sensitive microseismic monitoring arrays. In other cases, some preexisting faults under certain orientations and effective stress may get reacti-

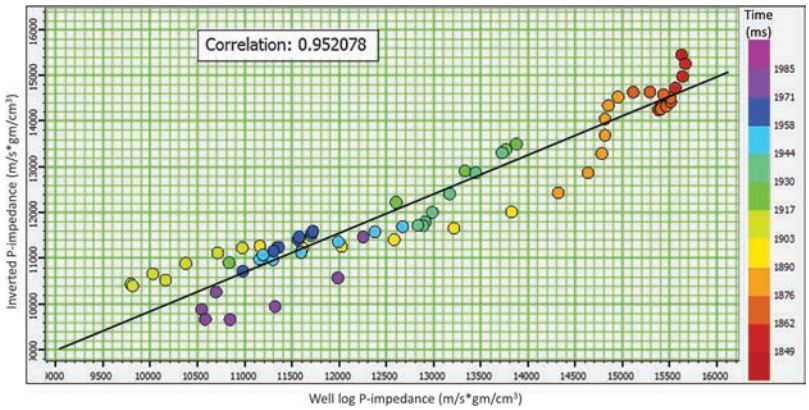

Figure 10. Correlation for well-log P-impedance and inverted P-impedance extracted at blind well W-3 for prestack joint inversion. The correlation coefficient is 0.95, which is very encouraging (data courtesy of Arcis Seismic Solutions, TGS, Calgary).

Table 1. Comparison of correlation coefficients evaluated from crossplots for P- and S-impedance from well-log data and inverted seismic data.

Well W-1	Simultaneous inversion	Poststack joint inversion	Prestack joint inversion
P-impedance	0.952420	0.931485	0.968957
S-impedance	0.945133	0.960941	0.977858

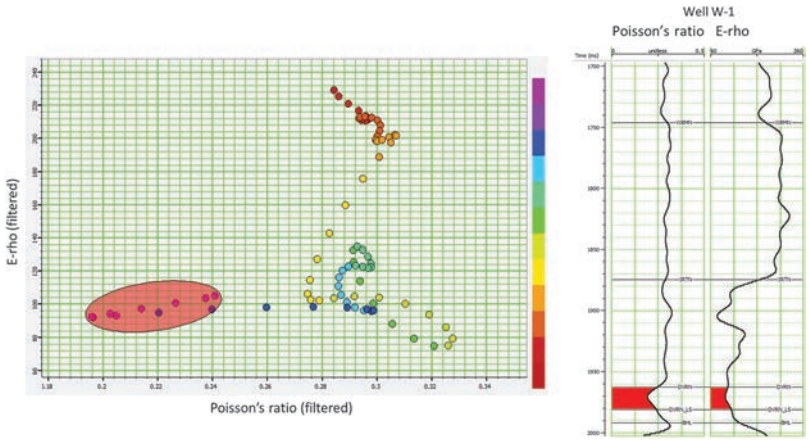

Figure 11. Crossplot between E-rho and Poisson's ratio for well W-1 broadly covering the Duvernay interval. The cluster of points enclosed by the red polygon appears to be anomalous and its back projection to the well-log curves shows that it highlights the Duvernay zone (data courtesy of Arcis Seismic Solutions, TGS, Calgary).

vated. In such cases, the magnitudes can increase to the level recordable by "induced seismicity" monitoring.

All these observations are suggestive that the seismic data should be extensively examined for the indications of faults and fractures. An initial straightforward approach is to determine discontinuities in the 3D seismic data volume by way of coherence, curvature, and brittleness (or other) attribute volumes. This was performed, but the initial strat-cube analysis at the Duvernay level, shown in Figure 13, showed no visible indication of any significant faults or fractures on the coherence displays. The curvature displays do indicate a few lineaments, which can be further studied for any possible connection with fault reactivation. At the present time, a complete study has not been carried out, but additional efforts are being made in that direction.

To take this analysis forward, we overlaid some data available from the Repsol-induced seismicity database on the brittleness and curvature displays as shown in Figure 14. Repsol has four seismometer stations in the area that are continuously recording the seismicity. Interestingly, the seismicity patterns do seem to fall close to the highbrittleness-index pockets. However, there seems to be no strong correlation of the events with curvature.

Over the past couple of years, three horizontal wells have been drilled from the same pad as shown on the displays in Figure 14. The two horizontal wells to the north drilled from the same pad (separation 200 m) were zipper fracked, and an event of magnitude 3.8 Mw was recorded on 23 January 2015. Interestingly, this and most events were recorded after completion of the frac and during or after fluid flow back. The horizontal well to the south was drilled from the same pad, and an event was recorded with a magnitude 4.1 Mw on 12 January 2016. The event happened suddenly when a particular completion stage was being fracked. As per the AER directives, work on the well had to be suspended immediately and before any flow back could be initiated. Some low-magnitude after-shock seismicity events continued to be recorded for several months. What this suggests is that perhaps pore pressure diffusion and strain transfer have a role in the fault reactivation in the broad zone around the completion, giving rise to seismicity.

The next question that comes to mind is about the depth(s) from which the large seismicity events originated. For the large event to the north, the hypocenter was estimated at a 5.4 km depth, and for the large event to the south, it was estimated to be at a 4.2 km depth. The Duvernay Formation is at a 3.4 km depth, and the basement is another 500 m below this level. So, the estimated depth of the event at 5.4 km is well below the basement. Apparently, for the surface seismometers, the error bars for the depth estimation are in excess of several hundred meters, and thus, a more accurate method may be required for depth estimation, such as microseismic monitoring, if we are going to under-

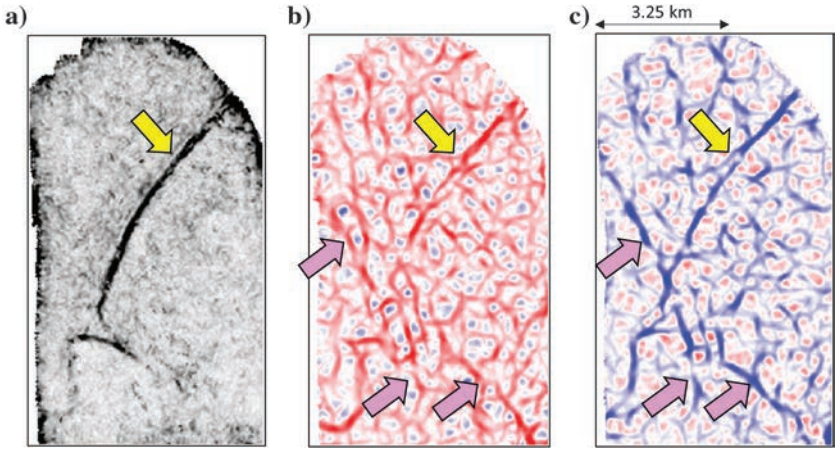

Figure 13. Horizon slice from (a) coherence volume, (b) most-positive curvature (long-wavelength), and (c) most-negative curvature (long-wavelength), 14 ms above the "Swan Hills" marker. The yellow arrow indicates the Swan Hills trend on the three attribute displays that are indicative of the termination of this facies along this trend. The pink arrows indicate other lineaments that need to be picked up for interpretation (data courtesy of Arcis Seismic Solutions, TGS, Calgary).

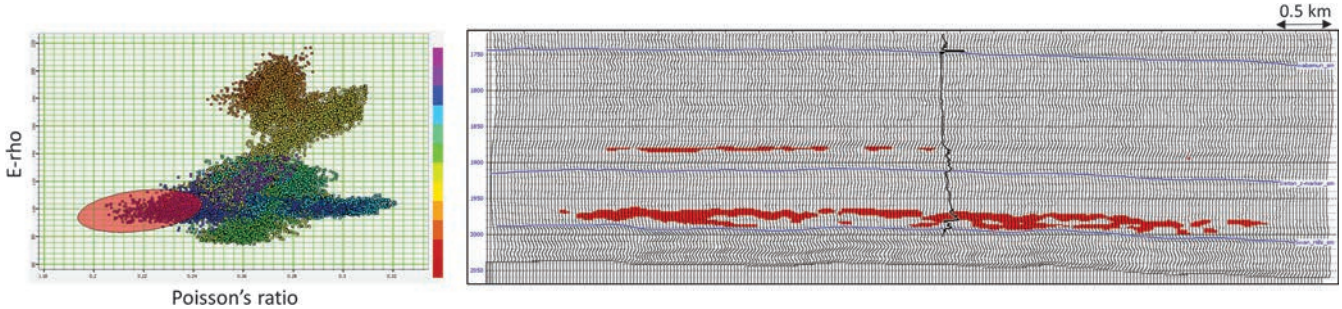

Figure 12. Crossplot of E-rho versus Poisson's ratio attributes derived from P- and S-impedance values derived using prestack joint inversion for data selected along line passing through well W-1. The cluster of points enclosed by the red polygon on back projection to the vertical seismic highlights the Duvernay interval that should be brittle (data courtesy of Arcis Seismic Solutions, TGS, Calgary).

stand the mechanism for induced seismicity and its mitigation going forward.

The next step was indeed to carry out a microseismic survey (not shown here); this was done only for the well to the south during the approximately 10-day fracking operation in January 2016. For the well to the south, a few of the microseismic event clusters indicated a staggered lineation pattern along the length of the horizontal segment with an orientation between the north and northeast, and more importantly coming from levels approximately 500 m above the Duvernay to approximately 100 m below it. Even if we assign an error bar of 100 m or so to the microseismic measurements, these results can be trusted, and efforts can be made to understand their origin.

When the microseismic data are overlaid/correlated (not shown) with the seismic data, no faults or fracture signatures are visible that could be readily correlated with the individual clusters above and below the horizontal well. But the staggered north-northeast pattern of the microseismic clusters along the length of the horizontal segment appears to be authentic in terms of their interpretation and comparison with other cases. This prompts us to conclude that if such signatures are not visible on the seismic, it does not mean that they are not there. Perhaps the seismic data need higher frequency content, or fresh seismic data with very small bin size need to be acquired so that somehow we get the detail we are looking for. Or perhaps the faults are strike slip with very little throw.

We went a step ahead and boosted up the frequency content of surface seismic using thin-bed reflectivity inversion (Chopra et al., 2006) and generated a volume of thin-bed reflectivity filtered back to a bandwidth of 10–15–150–160 Hz that is much higher as seen on the seismic displays in Figures 15 and 16. Coherence and curvature attributes were again computed on the frequency-enhanced seismic data, and horizon slices were generated at the Swan Hills and Basement levels, and are shown in Figures 15–17. Noticeably, the lineaments seen on the frequency-enhanced seismic data are crisper and carry more detail. The induced seismicity data overlaid in Figure 17c seem to fall on many of these lineaments, which is encouraging; but it is puzzling that other immediately adjacent, seemingly stronger, lineaments are not apparently related with seismicity.

At the present time, the microseismicity data have not been released for the close investigation that we are engaged in, but going forward, as it becomes available, it would be interesting to correlate it with the fault/fracture lineaments and try to explain their reactivation at different depths.

We recall some of the current available information that can help put the present exercise into perspective. Eaton et al. (1995) discuss about seismic evidence supporting basement controls on deposition and/or diagenesis in and around the area of our investigation. In the Kaybob South and Fox Creek areas, seismic evidence and detailed log marker correlation indicate two main northwest–southeast-trending normal faults cut the reservoir adjacent to an up-dip deep marine channel. Brecciation and fracturing occurred adjacent to these faults and thus appear to be related to faulting and hydrothermal dissolution.

Mountjoy et al. (1999) discuss the dolomitization in the deep basin of west-central Alberta including Kaybob

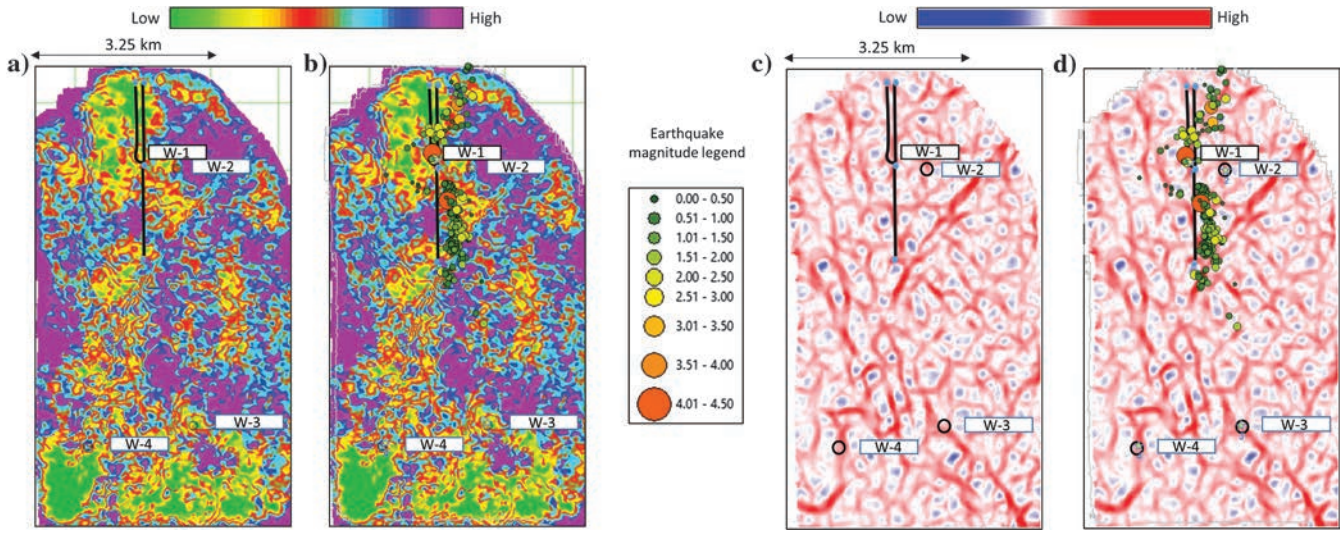

Figure 14. (a) Horizon slice from the brittleness coefficient averaged within the Duvernay zone. In (b), the induced seismicity events recorded by the seismic networks are overlaid. Events with magnitudes of less than 2 are in green, yellow represents events with magnitudes of 2 and above, and the two shades of orange represent magnitude greater than 3. Notice that most of the circles fall in those areas on the brittleness coefficient display that are in purple/blue, or pockets that are highly brittle. Horizon slice from the most-positive curvature (long-wavelength) volume 14 ms above the Swan Hills marker is shown in (c), and in (d) is the same slice as in (c) but with the seismicity events overlaid. Most of the faults seem to fall on lineaments exhibited on the positive curvature. The seismicity events are from the Repsol network database (data courtesy of Arcis Seismic Solutions, TGS, Calgary).

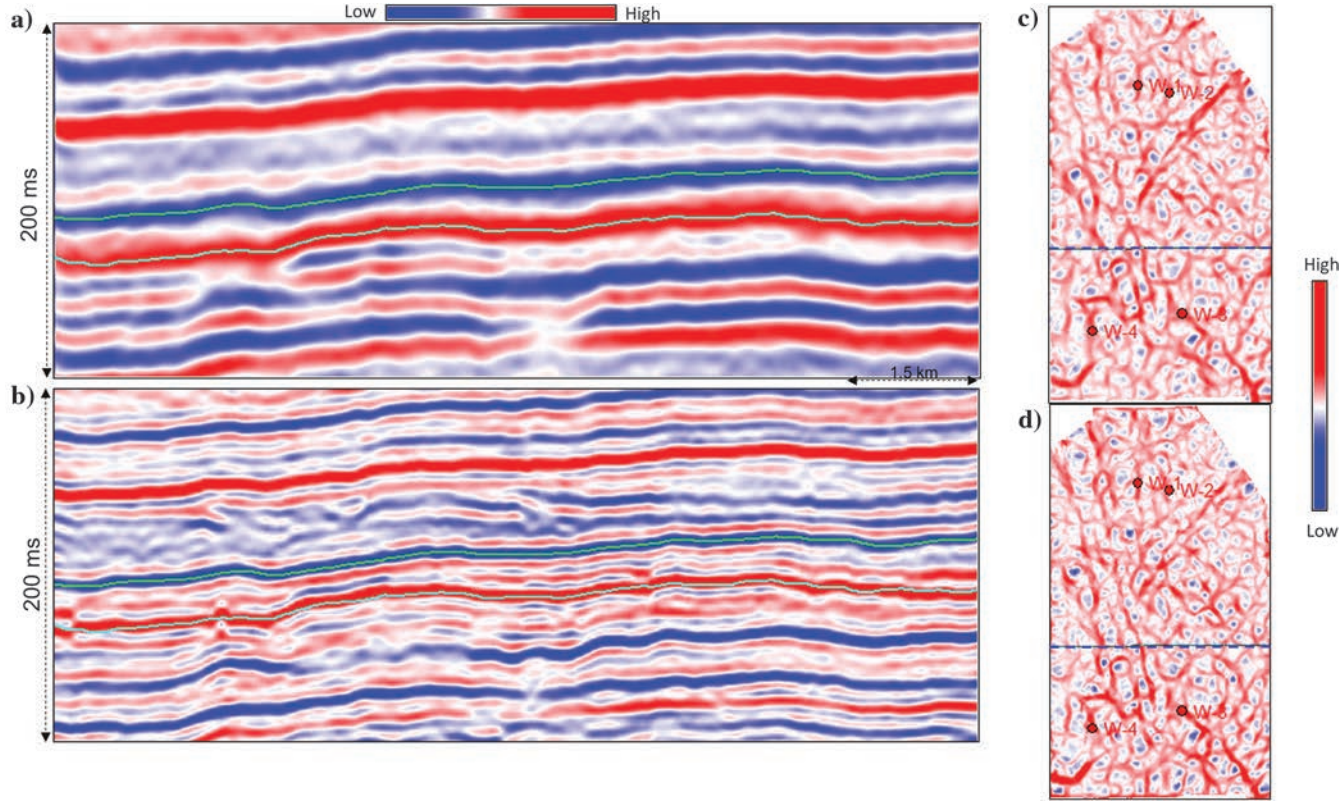

Figure 15. Equivalent segments of seismic sections from (a) input 3D seismic data and (b) filtered thin-bed reflectivity volume (10–15–150–160 Hz). Horizons slices at the Swan Hills level from the most-positive curvature computed on the (c) input 3D seismic data and (d) the filtered thin-bed reflectivity volume. A somewhat crisp and distinct definition of the lineaments is seen in (d) (data courtesy of Arcis Seismic Solutions, TGS, Calgary).

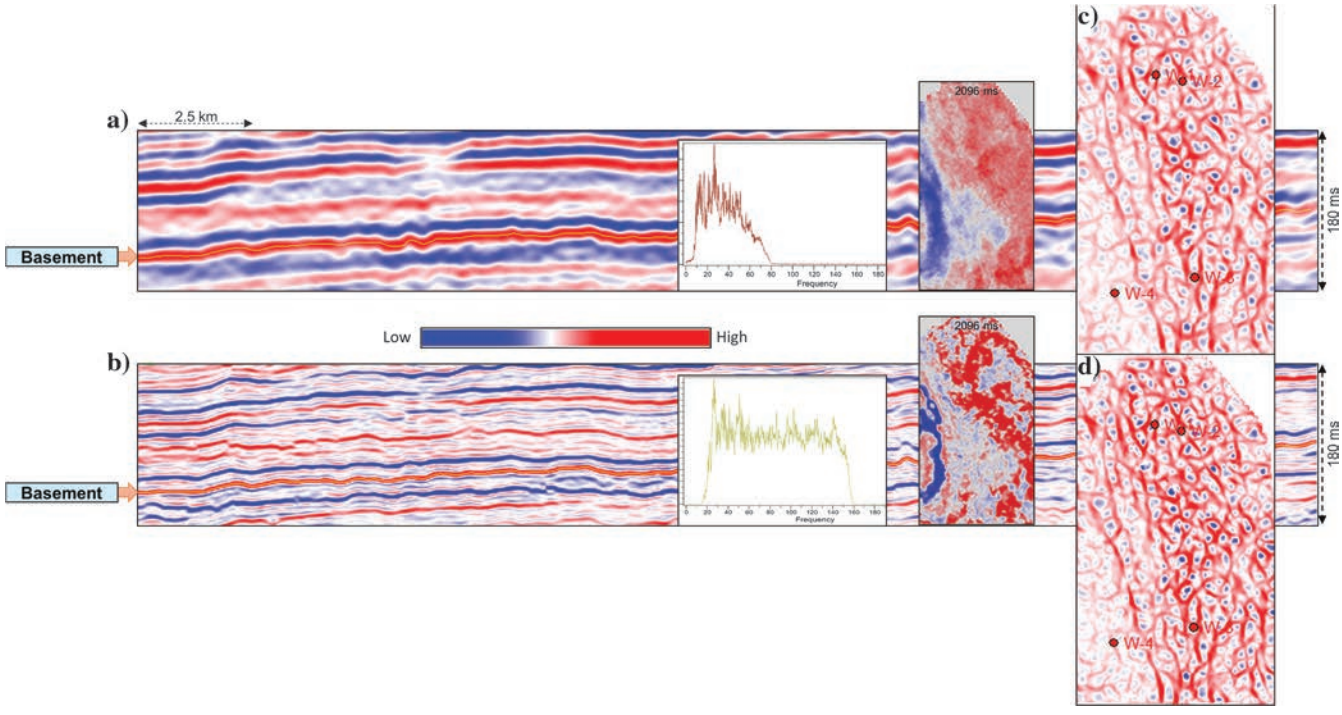

Figure 16. Equivalent segments of seismic sections from (a) input 3D seismic data and (b) filtered thin-bed reflectivity volume (10–15–150–160 Hz). Overlaid on the displays are the frequency spectra as well as the time slices at 2096 ms, which is the time level of the basement. Horizons slices at the basement level from the most-positive curvature computed on the (c) input 3D seismic data and (d) the filtered thin-bed reflectivity volume. Somewhat crisp and a distinct definition of the lineaments are seen in (d) (data courtesy of Arcis Seismic Solutions, TGS, Calgary).

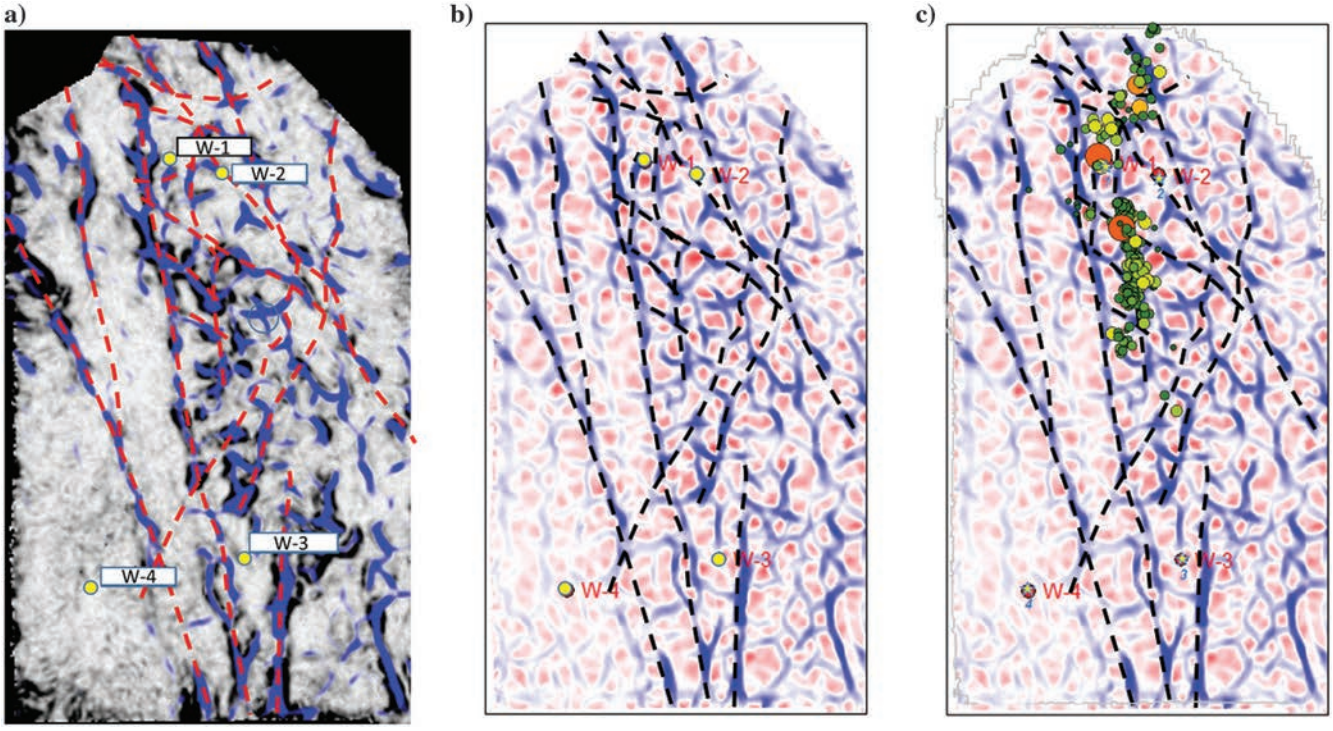

Figure 17. Horizons slices at the basement level from (a) coherence volume with most negative curvature volume merged with it using transparency and (b) most-negative curvature volume. Lineaments in red have been tracked on the display in (a) and shown in black on the display in (b). The induced seismicity points overlaid on the display in (c). Notice that many of these points fall on the black lineaments.

South and Fox Creek fields from the Swan Hills, Leduc, and Wabamun stratigraphic levels. The dolomitization around these areas probably occurred during deep burial (5–7 km) with hot fluids comprising connate brines and hydrothermal fluids, inferred to have been expelled from the Rocky Mountain fold thrust beds during the Laramide Orogeny. Schultz et al. (2016) note statistically significant association between the Swan Hills Formation and induced earthquakes and basement-controlled faults via reactivation.

As per Atkinson et al. (2016), there are no validated predictive models available, which can be used to assess the likelihood, rates, or the magnitudes of induced events from specific operations. The available models of induced seismicity are largely statistical in nature and rely on induced events above a certain magnitude on a per well basis. The authors find a level of correlation between the recorded seismicity and HF in space and time. This correlation is unlikely to be associated with nearby disposal wells. The conceptual model here is that diffusion of pore pressures is caused by HF, without going into the causative details of such a correlation.

In the above discussion, whatever may be the cause of the seismicity induced by the HF, the fact remains that the Duvernay Formation pockets, which are brittle, fracture better, and this has been determined using seismic attributes. The seismic attributes computed on frequency-enhanced seismic data hold promise in highlighting crisp lineament detail. The results presented here will benefit from further integration with additional work such as depth imaging, microseismic, azimuthal analysis, image logs, and geomechanical studies.

Conclusions

We have carried out seismic reservoir characterization of the Duvernay shale Formation in the Fox Creek area of Alberta, using multicomponent seismic data. The seismic attributes derived therefrom have enabled us to integrate the available induced seismicity data and attempt to draw some valid conclusions. Although it would be nice to conclude that there is strong correlation between derived brittleness, curvature, or other attributes and the resulting "fracability" or production, it is possible that overriding factors, such as involved fractures stealing away HF energy, have a larger effect than facies, brittleness sweet spots, or other seismically derivable attribute-related measures. Nonetheless, high-quality characterization investigations must be performed.

Questions about the depth accuracy of the induced seismicity data also remain, in view of the microseismic data that have been acquired for the one horizontal well. It remains important to correlate all available information with any seismic attributes work. Attributes computed on frequency-enhanced seismic data seem enticing.

We make the case that surface seismic data together with its integration with other relevant data can help characterize the Duvernay shale Formation.

Acknowledgments

We wish to thank the processing team at Arcis for their diligent efforts in delivering good-quality data in a timely fashion. We also wish to thank Repsol and Arcis Seismic Solutions, TGS, Calgary for permission to present this work.

References

Alberta Energy Regulator (AER), 2016, Seismicity in Alberta, https://www.aer.ca/about-aer/spotlight-on/seismicity-in-alberta, accessed 19 February 2016.

Atkinson, G. M., D. W. Eaton, H. Ghofrani, D. Walker, B. Cheadle, R. Schultz, R. Shcherbakov, K. Tiampo, J. Gu, R. M. Harrington, Y. Liu, M. V. der Baan, and H. Kao, 2016, Hydraulic fracturing and seismicity in the Western Canada Sedimentary Basin: Sedimentological Research Letters, **87**, 631–647, doi: 10.1785/0220150277.

Chopra, S., 2015, The buzz about quantitative seismic interpretation: Presented at the Arcis Symposium.

Chopra, S., J. P. Castagna, and O. Portniaguine, 2006, Seismic resolution and thin-bed reflectivity inversion: CSEG Recorder, **31**, 19–25.

Chopra, S., and R. K. Sharma, 2015, Impedance inversion: Big aid in interpretation: AAPG Explorer, **36**, 34–35.

Chopra, S., and R. K. Sharma, 2016, Preconditioning of seismic data prior to impedance inversion: AAPG Explorer, **37**, 30–33.

Eaton, D. W., B. Milkereit, G. M. Ross, E. R. Kanasewich, W. Geis, D. J. Edwards, L. Kelsch, and J. Varsek, 1995, Lithoprobe basin-scale seismic profiling in central Alberta: Influence of basement on the sedimentary cover: Bulletin of Canadian Petroleum Geology, **43**, 65–77.

Greiser, B., and J. Bray, 2007, Identification of production potential in unconventional reservoir: SPE 106623: Presented at the SPE Production and Operations Symposium.

Hunt, L., P. Cary, D. Tican, M. Perz, R. K. Sharma, N. Nagarajappa, X. Li, and S. Chopra, 2015, VOQC: Value oriented quality control in seismic processing: CSEG Recorder, **40**, 42–51.

Kutchment, A., 2016, Drilling for earthquakes: Scientific American, **315**, 46–50, doi: 10.1038/scientificamerican0716-46.

Lawton, D. C., 1991, Source-receiver offset ranges for P-SV seismic data, CREWES Research Report, http://www.crewes.org/ForOurSponsors/ResearchReports/abstract.php?file=/ForOurSponsors/ResearchReports/1991/1991-03.pdf, accessed 15 February 2016.

Mountjoy, E. W., H. G. Machel, D. Green, J. Duggan, and A. E. Williams-Jones, 1999, Devonian matrix dolomites and deep burial carbonate cements: A comparison between the Rimbey-Meadowbrook reef trend and the deep basin of west-central Alberta: Bulletin of Canadian Petroleum Geology, **42**, 487–509.

Mossop, G. D., and I. Shetsen, 1994, Geological atlas of the Western Canada sedimentary basin: Canadian Society of Petroleum Geologists and Alberta Research Council, http://www.ags.gov.ab.ca/publications/wcsb_atlas/atlas.html, accessed 15 August 2016.

Ray, A. K., and S. Chopra, 2015, More robust methods of low-frequency model building for seismic impedance inversion: 85th Annual International Meeting, SEG, Expanded Abstracts, 3398–3402.

Ray, A. K., and S. Chopra, 2016, Building more robust low-frequency models for seismic impedance inversion: First Break, **34**, 29–34.

Schultz, R., H. Corlett, K. Haug, K. Kocon, K. MacCormack, V. Stern, and T. Shipman, 2016, Linking fossil reefs with earthquakes: Geologic insight to where induced seismicity occurs in Alberta: Geophysical Research Letters, **43**, 2534–2542, doi: 10.1002/2015GL067514.

Sharma, R. K., and S. Chopra, 2015, Determination of lithology and brittleness of rocks with a new attribute: The Leading Edge, **34**, 554–564, doi: 10.1190/tle34050554.1.

Weingarten, M., S. Ge, J. W. Godt, B. A. Bekins, and J. L. Rubenstein, 2015, High-rate injection is associated with the increase in U.S. mid-continent seismicity: Science, **348**, 1336–1340, doi: 10.1126/science.aab1345

Satinder Chopra has 33 years of experience as a geophysicist specializing in processing, reprocessing, special processing, and interactive interpretation of seismic data. He has rich experience in processing various types of data such as VSP, well-log data, and seismic data. He has been the 2010/11 CSEG distinguished lecturer, the 2011/12 AAPG/SEG distinguished lecturer, and the 2014/15 EAGE e-distinguished lecturer. He has published eight books and more than 380 papers and abstracts. His work and presentations have won several awards, the most notable ones being the CSEG Honorary Membership (2014) and Meritorious Service (2005) Awards, 2014 Association of Professional Engineers, Geologists and Geophysicists of Alberta (APEGA) Frank Spragins Award, the 2010 AAPG George Matson Award, the 2013 AAPG Jules Braunstein Award, SEG Best Poster Awards (2007, 2014), and CSEG Best Luncheon Talk (2007). He is a member of SEG, CSEG, CSPG, EAGE, AAPG, and APEGA. His research interests focus on techniques surrounding the characterization of reservoirs.

Ritesh Kumar Sharma received a master's (2007) in applied geophysics from the Indian Institute of Technology, Roorkee, India, and received an M.S. (2011) in geophysics from the University of Calgary. He works as an advanced reservoir geoscientist at Arcis Seismic Solutions, TGS, Calgary. He is involved in deterministic inversions

of poststack, prestack, and multicomponent data in addition to AVO analysis, thin-bed reflectivity inversion, and rock-physics studies. Before joining the company in 2011, he served as a geophysicist at Hindustan Zinc Limited, Udaipur, India. He won the best poster award for his presentation titled "Determination of elastic constants using extended elastic impedance," at the 2012 GeoConvention held at Calgary. He also received the Jules Braunstein Memorial Award for the best AAPG poster presentation titled "New attribute for determination of lithology and brittleness," at the 2013 AAPG Annual Convention and Exhibition held in Pittsburgh. He has received CSEG Honorable Mention for the Best Recorder Paper award in 2013. He is an active member of SEG and CSEG.

Amit Kumar Ray received an M.S. in geophysics from Indian School of Mines, India. He works as a geophysicist at Gujarat Energy Research and Management Institute, India. He was previously at Arcis Seismic Solutions, TGS in Calgary as a reservoir geoscientist. Prior to that, he has worked in Gujarat State Petroleum Corporation Ltd., Reliance Industries Ltd., and the Centre for Development of Advanced Computing in India in various geophysical positions. He has 12 years of experience in the oil and gas industry. He has been primarily working in the areas of seismic reservoir characterization, 2D/3D seismic interpretation, AVO/AVA analysis and inversion, and multiattribute analysis and neural networks.

M. Hossein Nemati received B.S. and M.S. degrees in petroleum exploration engineering from Iran and received an M.S. in integrated petroleum geosciences from the University of Alberta. He is a geoscientist at Arcis/TGS in Calgary and works on the subsurface evaluation and interpretation and supports multiclient business. Due to his dual background, he has been working in different areas from exploration to field development projects such as G&G interpretation, reservoir modeling, and petrophysics. His recent work has been focused on a variety of plays in basins across North America, including unconventionals. He is a member of AAPG, SPE, CSEG, and CSPG.

Ray Morin received a B.S. (1999) in geophysics from the University of Calgary. He is a geophysicist at Repsol Oil & Gas Canada. In his current role, he is working in the Fox Creek region of central NW Alberta. He joined Talisman Energy in 2000, which was then acquired by Repsol in 2016. He is an active member of CSEG and APEGA.

Brian Schulte received a B.S. (1989) in geology with a minor in geophysics from the University of Calgary when he subsequently entered into the oil industry. Since then, he has had a long and winding career and traveled around the world working in seismic processing, acquisition, interpretation, rock physics, and petrophysics. He volunteers as an advisor for the CSEG Emerging Professionals Program and has presented and written papers on AVO, seismic interpretation, and seismic processing in numerous publications and at various geophysical forums. He works for Repsol as a geophysical advisor working on projects associated with quantitative interpretation, quality assurance, mentorship, and technical developments.

David D'Amico received a B.S. (1984) (honors) in physics and an M.S. (1986) (medical imaging) in physics from the University of Alberta, Edmonton, Canada. He is a manager, Geoscience, North American Subsurface Development for Repsol Oil & Gas Canada Inc. He started his career with Amoco Canada where he received excellent grounding in all aspects of geophysics. For a few years, he was a manager of geophysics at a small startup exploration company where for a time he was the only geophysicist and had to do it all. This was prior to joining Talisman Energy Inc. in 2002, where he has enjoyed working on many interesting projects around the globe, including coordinating peer reviews for risking and volumetrics for all Talisman exploration wells worldwide. He leads a technical team supporting development groups with pragmatic solutions to geoscience problems. He is interested in improving technical collaboration and integration among groups.